Response spectrum of coupled nanomechanical resonators

J. Dorignac,[1] A. Gaidarzhy,[1,a)] and P. Mohanty[2]
[1]*College of Engineering, Boston University, Boston, Massachusetts 02215, USA*
[2]*Department of Physics, Boston University, Boston, Massachusetts 02215, USA*

(Received 21 May 2008; accepted 19 August 2008; published online 10 October 2008)

We develop a simple *continuum* model to analyze the vibrational modes of a nanomechanical multielement structure. In this model, arrays of submicron cantilevers located symmetrically on both sides of the central clamped-clamped nanobeam are replaced by a continuum. In this approach, the equations of motion of the structure become exactly solvable. Our analytical results capture the main features of the vibrational modes observed both numerically and experimentally and can be applied to a general class of scale-independent elasticaly coupled resonator structures. © *2008 American Institute of Physics*. [DOI: 10.1063/1.2996031]

I. INTRODUCTION

Nanomechanical resonators have been used to investigate fundamental physics problems in a wide range of research areas. These include quantum measurement and quantum computation,[1–5] ultrasensitive force and mass detection,[6] electronic spin detection and manipulation,[7] gravitational wave detection[4,5] and other fundamental phenomena.[8–11] The central reason for the increasing interest and activity in nanomechanical systems for quantum studies is straightforward: Fast dynamics of nanomechanical systems enable the investigation of the yet-unexplored corner of the parameter space where ultrahigh frequency resonance modes cooled to near-zero temperatures are expected to manifest quantum mechanical corrections to the classical motion.[12–14]

Likewise, from a technological standpoint, compact size, robustness, and high frequencies of nanomechanical resonators have resulted in numerous proposals for applications where technologies involving nanomechanical systems can offer alternative solutions to the existing electronic circuits and off-chip devices: frequency selective oscillators,[15] passive filters,[16] memory elements,[17] and spintronics devices.[18] The driving force behind micro- and nanoelectromechanical systems (MEMS and NEMS) has been the portfolio of MEMS applications in optical communication (routers, switches, repeaters), passive devices in cellphone industry (filters, accelerometers, capacitors, and inductors for integrated chip design), and sensor technologies in chemical, biomedical, and electrical solutions. Nanomechanical structures are faster (because of higher resonance frequencies) and can be orders of magnitude smaller than the existing technologies. In fact, the range of frequencies discussed in this paper matches with the frequency bands for communication in a number of consumer devices: cellular (0.4, 0.85, and 1.9 GHz), WiFi and bluetooth (2.4 GHz), satellite radio (~2.3 GHz), and global positioning system receivers (L1–L3: 1.2–1.6 GHz).

Since the structure size is reduced for increasing resonant mode frequencies—and hence the operation speed of the device—it is possible that within a few years certain applications with nanomechanical devices will emerge which will have frequencies high enough so that at the relevant operating temperatures the nanomechanical element will be quantum mechanical. A specific application of gigahertz-range nanomechanical oscillators involves space communication devices (0.5–18 GHz). As passive devices, nanomechanical structures in certain space communication applications are expected to remain at low temperatures, perhaps near the quantum regime. This leads to the obvious realization that further shrinkage of micro- or nanomechanical systems with corresponding high gigahertz-range frequencies will inevitably require new paradigms.

Central to many of the aforementioned applications of NEMS resonators is the attainment high natural frequencies of motion up to and beyond the 1 GHz mark. Among the various solutions proposed for achieving ultrahigh frequencies in nanomechanical resonators such as the use of high stiffness materials[19,20] and bulk mode geometries,[21] our approach of coupling mechanical elements to enhance high order resonant modes of the resonator structure has been shown to offer a number of advantages for performance and detection ease.[22] The coupling of additional degrees of freedom to a 10 μm long simple nanobeam structure can produce significant modification of the high order resonance spectrum, with enhanced amplitude and quality factors of selected vibration modes extending well beyond the 1 GHz frequency range.

Despite the broad areas of interest in nanomechanical systems, comprehensive studies of elasticity and mechanics of nanomechanical structures are yet to be done beyond the simple single-element structures such as cantilevers and clamped beams. A major difficulty has been the extension of elasticity theory to multielement structures for closed-form analytical solutions. As many of the applications of nanomechanical systems include complex structure design, analytical understanding of resonant modes and other dynamical aspects such as nonlinear mode coupling in complex multielement structures is of central importance.

For a comprehensive study of nanomechanical resonators, such devices need to be properly characterized for their elastic behavior. However, as system size shrinks down to the submicron or nanoscale, material properties become ato-

a)Electronic mail: alexei@bu.edu.

mistic rather than continuous, and this gives rise to a host of anomalous behaviors.[23] These include enhancement of influence of surface defects and crystal imperfections, quantum energy dissipation mechanisms, reduction in the effective stiffness constant, and statistical fluctuation effects. Modeling of structures too small for continuum mechanics and too large for atomistic molecular dynamics simulation requires a proper understanding of the coupling of length scales. Additionally, correlation of simulated modeshapes and experimentally measured modes will require the knowledge of relevant static and dynamic parameters. Therefore, analytical studies of complex nanomechanical systems will not only provide a strong motivation for new approaches to model materials beyond the current limit of computing capacity, they will augment the ongoing work on the multiscale modeling of fracture dynamics and nanomaterials.

Here, we present an elastic model that yields closed-form solutions describing the dynamics of the coupled-beam resonator, dubbed the antenna structure. This structure is a prototype of a class of two-element structures that has been envisioned in specific experimental applications.[20] The continuum model (CM) allows for a clear comparison of the modal shapes and spectrum with full finite element (FE) analysis of the structure. The model we derive is not scale specific. It can be applied to large or small scale structures provided that the basic requirements of elasticity theory are satisified. Although, for simplicity here, we treat the vibrations of the structure within the Euler–Bernouilli beam approximation, more sophisticated theories—such as Timoshenko theory—may be used as well.[24] Furthermore, nonlinear effects such as anharmonic modal coupling in such structures can be readily modeled by solving the corresponding nonlinear system of equations.[25] Finally, we note that our CM is quite general and can be readily extended to structures whose cantilevers have an arbitrary length profile and density along the central beam. These topics will be addressed in a forthcoming publication.

II. CONTINUUM MODEL

A. Discrete equations of motion

The nanomechanical resonating structure we investigate consists of a central clamped-clamped beam with dimensions $L\times W\times h=10.7\times 0.4\times 0.35$ μm^3 and 40 perpendicular cantilevers with dimensions $l\times w\times h=0.5\times 0.2\times 0.35$ μm^3. The cantilevers are regularly spaced along the beam and symmetric with respect to the beam (see Fig. 1). There are $N=20$ cantilevers on each side. In experimental applications, the top surface of the structure is typically coated with a thin layer of metal whose length and width are those of the beam and whose thickness is $t=0.035$ μm. We denote by x the coordinate along the beam and by ξ the transverse one. The deflection of the beam with respect to its clamps is called $y(x,t)$ and the deflection of the jth lateral cantilever with respect to $y(x_j,t)$ is denoted by $\eta_j(\xi,t)$. In the following we shall only consider vibrational modes *symmetric* with respect to the central beam. The deflection of the cantilevers on either side of the beam is thus $\eta_j(\xi,t)$. Considering that all the elements of the structure are one dimensional and using the

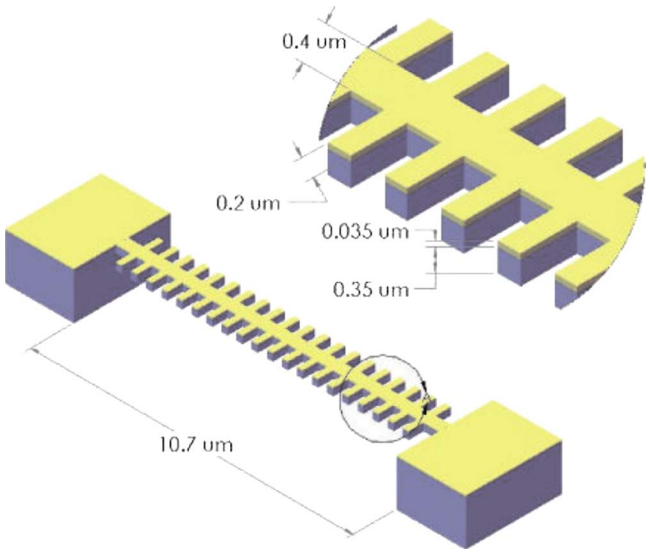

FIG. 1. (Color online) Coupled-element resonator structure.

Euler–Bernoulli beam theory (see for example Refs. 25–27), the equations of motion of the structure have the form

$$\mathcal{E}_b\frac{\partial^4 y}{\partial x^4}+\mu_b\frac{\partial^2 y}{\partial t^2}=-2\mathcal{E}_t\sum_{j=1}^{N}\left.\frac{\partial^3\eta_j}{\partial\xi^3}\right|_{\xi=0}\delta(x-x_j), \tag{1}$$

$$\mathcal{E}_t\frac{\partial^4\eta_j}{\partial\xi^4}+\mu_t\frac{\partial^2\eta_j}{\partial t^2}=-\mu_t\frac{\partial^2 y_j}{\partial t^2},\quad j\in\{1,\ldots,N\}, \tag{2}$$

where $y_j\equiv y(x_j,t)$ and together with the boundary conditions

$$y(0,t)=\frac{\partial y}{\partial x}(0,t)=y(L,t)=\frac{\partial y}{\partial x}(L,t)=0, \tag{3}$$

$$\eta_2(0,t)=\frac{\partial\eta_j}{\partial\xi}(0,t)=\frac{\partial^2\eta_j}{\partial\xi^2}(l,t)=\frac{\partial^3\eta_j}{\partial\xi^3}(l,t)=0, \tag{4}$$

with $j\in\{1,\ldots,N\}$. The rigidities of the beam, $\mathcal{E}_b$, and the cantilevers, $\mathcal{E}_t$, that account for the two material layers—here, nanocrystaline diamond and gold—are given, respectively, by (see, e.g., Ref. 27)

$$\mathcal{E}_b=\frac{W}{12}\frac{[E_d^2h^4+E_dE_g(4h^3t+6h^2t^2+4ht^3)+E_g^2t^4]}{(E_dh+E_gt)},$$

$$\mathcal{E}_t=\frac{w}{W}\mathcal{E}_b, \tag{5}$$

where $E_d=700$ GPa and $E_g=45.6$ GPa are the measured Young's moduli of diamond and gold, respectively. The masses per unit length of the beam and a cantilever are respectively given by

$$\mu_b=W(\rho_dh+\rho_gt),\quad \mu_t=\frac{w}{W}\mu_b, \tag{6}$$

where $\rho_d=4050$ kg m^{-3} and $\rho_g=19\,500$ kg m^{-3} are the densities of diamond and gold, respectively. It is important to note that because of the smallness of E_g with respect to E_d, the rigidities of the beam and the cantilever are barely affected by the presence of the gold layer (roughly 2.5%

higher). This is in contrast with their linear mass that the gold layer increases by roughly 50%. Thus, the presence of the gold layer merely increases the mass of the antenna without affecting its rigidity.

The force density in the right hand side of Eq. (1) represents the shear force densities exerted by the cantilevers on the beam. No momenta appear in this equation because for modes that are symmetric with respect to the central beam, the momenta exerted by two opposite cantilevers cancel each other. The right hand side of Eq. (2) is due to the motion of the base of the cantilever that follows the motion of the central beam at $\xi=0$.

B. Continuum approximation

We now derive a continuum approximation for the system of Eqs. (1)–(4). The idea is to "smooth out" the punctual force densities of Eq. (1) in such a way that the total shear force exerted by the jth cantilever on the beam is the same but with a density that is continuous along the beam. This basically amounts to replacing the discrete sum in the right hand side of Eq. (1) by an integral, which yields

$$\mathcal{E}_b \frac{\partial^4 y(x,t)}{\partial x^4} + \mu_b \frac{\partial^2 y(x,t)}{\partial t^2} = -\frac{2\mathcal{E}_t N}{L} \left.\frac{\partial^3 \eta(x,\xi,t)}{\partial \xi^3}\right|_{\xi=0}, \tag{7}$$

$$\mathcal{E}_t \frac{\partial^4 \eta(x,\xi,t)}{\partial \xi^4} + \mu_t \frac{\partial^2 \eta(x,\xi,t)}{\partial t^2} = -\mu_t \frac{\partial^2 y(x,t)}{\partial t^2}, \tag{8}$$

with clamped-clamped and cantileverlike boundary conditions for the central beam and the cantilevers, respectively,

$$y(0,t) = \frac{\partial y}{\partial x}(0,t) = y(L,t) = \frac{\partial y}{\partial x}(L,t) = 0, \tag{9}$$

$$\eta(x,0,t) = \frac{\partial \eta}{\partial \xi}(x,0,t) = \frac{\partial^2 \eta}{\partial \xi^2}(x,l,t) = \frac{\partial^3 \eta}{\partial \xi^3}(x,l,t) = 0. \tag{10}$$

Equations (7) and (8) conserve the following energy:

$$H_c = \int_0^L dx \left[\frac{\mathcal{E}_b}{2}\left(\frac{\partial^2 y}{\partial x^2}\right)^2 + \frac{\mu_b}{2}\left(\frac{\partial y}{\partial t}\right)^2\right] + \frac{2N}{L}\int_0^L dx \int_0^l d\xi \left[\frac{\mathcal{E}_t}{2}\left(\frac{\partial^2 \eta}{\partial \xi^2}\right)^2 + \frac{\mu_t}{2}\left(\frac{\partial \eta}{\partial t} + \frac{\partial y}{\partial t}\right)^2\right]. \tag{11}$$

The CM presented above becomes more accurate as the density of cantilevers, N/L, increases. To get a sense of its limitations, let us imagine that for a given mode, the shape of the central beam has $n-1$ nodes, and consequently n antinodes. We then expect the model to hold if at least one cantilever per antinode subsists, which yields the following condition of validity for the CM:

$$n < N. \tag{12}$$

Indeed, if condition (12) was not satisfied, the "cantilever continuum" would create some inertial effects on an antinode where no physical cantilever is present, which is not desirable. The limit of a single cantilever per arch, instead of two or more, can still appear rather arbitrary. However a comparison of the lower part of the spectrum of the continuum and discrete models for $N=1$ reveals that their first frequencies are very similar. Therefore, thinking of the central beam as a collection of subbeams (antinodes) pinned at the level of its nodes, it seems reasonable to take one cantilever per antinode as the limit of validity of the CM.

C. Vibrational modes

Defining the following nondimensional quantities

$$u = \frac{x}{L}, \quad v = \frac{\xi}{l}, \quad \mu^4 = \frac{\mu_b L^4 \omega^2}{\mathcal{E}_b}, \quad \gamma^4 = \frac{\mu_t l^4 \omega^2}{\mathcal{E}_t}, \quad R = 2\left(\frac{L}{l}\right)^3 \frac{\mathcal{E}_t}{\mathcal{E}_b}, \tag{13}$$

we look for mode solutions of the form

$$y(x,t) = Y(u)\cos(\omega t), \quad \eta(x,\xi,t) = H(u,v)\cos(\omega t). \tag{14}$$

The equations of motions (7) and (8) become

$$\frac{d^4 Y(u)}{du^4} - \mu^4 Y(u) = -RN \frac{\partial^3 H}{\partial v^3}(u,0), \tag{15}$$

$$\frac{\partial^4 H(u,v)}{\partial v^4} - \gamma^4 [H(u,v) + Y(u)] = 0, \tag{16}$$

with boundary conditions

$$Y(0) = \frac{dY}{du}(0) = Y(1) = \frac{dY}{du}(1) = 0, \tag{17}$$

$$H(u,0) = \frac{\partial H}{\partial v}(u,0) = \frac{\partial^2 H}{\partial v^2}(u,1) = \frac{\partial^3 H}{\partial v^3}(u,1) = 0. \tag{18}$$

Now, solving Eq. (16) yields

$$H(u,v) = [A_1(\gamma)\cos(\gamma v) + A_2(\gamma)\sin(\gamma v) + A_3(\gamma)\cosh(\gamma v) + A_4(\gamma)\sinh(\gamma v) - 1]Y(u) \equiv \hat{H}(v)Y(u), \tag{19}$$

where the coefficients $A_i(\gamma)$, determined by the boundary condition (18), are given by

$$A_1(\gamma) = \frac{1 + \cos\gamma\cosh\gamma - \sin\gamma\sinh\gamma}{2(1+\cos\gamma\cosh\gamma)},$$

$$A_2(\gamma) = \frac{\cos\gamma\sinh\gamma + \sin\gamma\cosh\gamma}{2(1+\cos\gamma\cosh\gamma)},$$

$$A_3(\gamma) = \frac{1 + \cos\gamma\cosh\gamma + \sin\gamma\sinh\gamma}{2(1+\cos\gamma\cosh\gamma)},$$

$$A_4(\gamma) = -\frac{\cos\gamma\sinh\gamma + \sin\gamma\cosh\gamma}{2(1+\cos\gamma\cosh\gamma)}. \tag{20}$$

From these results we can calculate the right hand side of Eq. (15), $-RN\partial^3 H/\partial v^3(u,0) = 2RN\gamma^3 A_2(\gamma)Y(u)$, and we finally obtain

$$\frac{d^4Y(u)}{du^4} - \beta^4 Y(u) = 0, \tag{21}$$

with

$$\beta^4 = \mu^4 + \gamma^3 RN \frac{\cos\gamma \sinh\gamma + \sin\gamma \cosh\gamma}{1 + \cos\gamma \cosh\gamma}. \tag{22}$$

Equations (21) and (22) show that our CM reduces to a simple clamped-clamped beam equation with a parameter β that depends in a nontrivial way upon the mode frequency ω. Indeed, according to Eq. (13), the parameters μ^4 and γ^4 are quadratic functions of the frequency and the parameters R and N are simply constants. Now, because Eq. (21) along with boundary condition (17) is merely a clamped-clamped beam equation, it can be solved to obtain

$$Y(u) = A\left\{\cos(\beta u) - \cosh(\beta u) - \left(\frac{\cos\beta - \cosh\beta}{\sin\beta - \sinh\beta}\right) \times [\sin(\beta u) - \sinh(\beta u)]\right\}, \tag{23}$$

with the secular equation

$$\cos(\beta)\cosh(\beta) = 1. \tag{24}$$

III. FREQUENCY SPECTRUM OF THE CONTINUUM MODEL

A. Band structure

We see that the shape of the vibrational modes of the central beam is uniquely determined by the parameter β solution to Eq. (24). The solutions β_n can be evaluated numerically: $\beta_1 = 4.730\,040\,745$, $\beta_2 = 7.853\,204\,624$, $\beta_3 = 10.995\,607\,84$, and $\beta_n \simeq (n+1/2)\pi$ as n is large. To a given β_n corresponds a single modal shape for the central beam, $Y_n(u)$, but an infinite number of modal shapes $H_{n,k}(u,v)$ and frequencies $\omega_{n,k}$, $k \geqslant 1$, obtained by solving Eq. (22) for ω. To see that the number of solutions to Eq. (22) for $\beta = \beta_n$ is infinite, we first rewrite it in terms of the variable γ by using $\mu = \gamma L/l$ and denoting by $m_b = L\mu_b$ and $m_t = l\mu_t$ the masses of the beam and of one cantilever, respectively, we finally find

$$Q(\gamma, \beta_n) \equiv \left(\cos\gamma + \frac{1}{\cosh\gamma}\right)\left[1 - \left(\frac{l\beta_n}{L\gamma}\right)^4\right] + \frac{2Nm_t}{m_b}\frac{\cos\gamma \tanh\gamma + \sin\gamma}{\gamma} = 0, \tag{25}$$

valid for $\cos\gamma\cosh\gamma + 1 \neq 0$. It now becomes clear that when γ is large, Eq. (25) reduces to $\cos\gamma = 0$. This equation has an infinite number of solutions with asymptotic behavior $\gamma_{n,k} = (k - 1/2)\pi$ as $k \to \infty$. Interestingly, these asymptotic solutions are independent of all the parameters entering Eq. (25), and in particular, of β_n *provided the latter is finite*, i.e., $n \to \infty$. Finally, the frequency corresponding to a given value $\gamma_{n,k}$ is given by Eq. (13) as

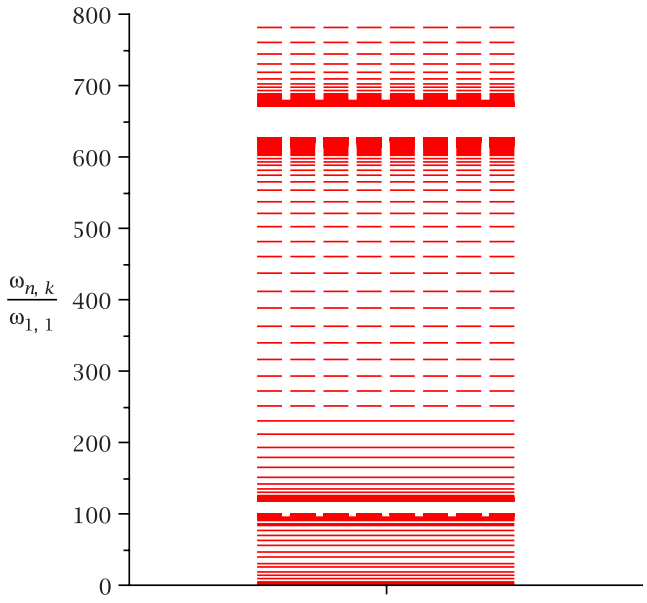

FIG. 2. (Color online) Frequency spectrum obtained from Eq. (25) for $N = 20$ and the antenna parameters given in Sec. II A. Solid lines correspond to $n < N$ (physically relevant frequencies) and dashed ones to $n > N$.

$$\omega_{n,k} = \sqrt{\frac{\mathcal{E}_t}{\mu_t}}\left(\frac{\gamma_{n,k}}{l}\right)^2. \tag{26}$$

To understand the structure of the spectrum, we have plotted in Fig. 2 the frequencies $\omega_{n,k}$ normalized to the fundamental, $\omega_{1,1}$, for $N = 20$ and the antenna dimensions indicated in Sec. II A. As we can see, the spectrum consists of "bands" separated by gaps. The band number is the label k that we have attributed to the solution of Eq. (25), $\gamma_{n,k}$. To elucidate the appearance of bands, we note that as n increases, the solution to Eq. (24) becomes large and is asymptotically given by $\beta_n \sim (n+1/2)\pi$. For a finite solution, $\gamma_{\infty,k}$, of Eq. (22) to exist as $n \to \infty$, the denominator of the second term of the right hand side of Eq. (22) needs to vanish. Hence,

$$1 + \cos(\gamma_{\infty,k})\cosh(\gamma_{\infty,k}) = 0. \tag{27}$$

This equation is the well-known secular equation for a simple cantilever. It provides here the upper band edge of the kth band whose frequency, determined by Eq. (26), reads

$$\omega_{\infty,k} = \sqrt{\frac{\mathcal{E}_t}{\mu_t}}\left(\frac{\gamma_{\infty,k}}{l}\right)^2. \tag{28}$$

For the case at hand, we have $\omega_{\infty,1}/\omega_{1,1} \simeq 100.103$, $\omega_{\infty,2}/\omega_{1,1} \simeq 627.336$, and $\omega_{\infty,k}/\omega_{1,1} \simeq [(k-1/2)\pi/\gamma_{1,1}]^2$ with $\gamma_{1,1} \simeq 0.187\,413$ for $k \geqslant 3$. It is easy to see that the accuracy of the latter formula improves exponentially as k increases. For $k = 3$ the relative error to the exact result is already as small as 0.02%. An approximate analytical expression for $\gamma_{1,1}$ is given in the next section while results for the lower edge of the kth band, $\gamma_{1,k}$, $k \geqslant 2$, will be given in Sec. III C.

At the edges of each band but the lower edge of the first one that we shall refer to as the "fundamental band," frequencies clearly accumulate. However, close to the lower band edge, a finite number of frequencies cluster while an infinite number accumulate at the upper band edge. Each

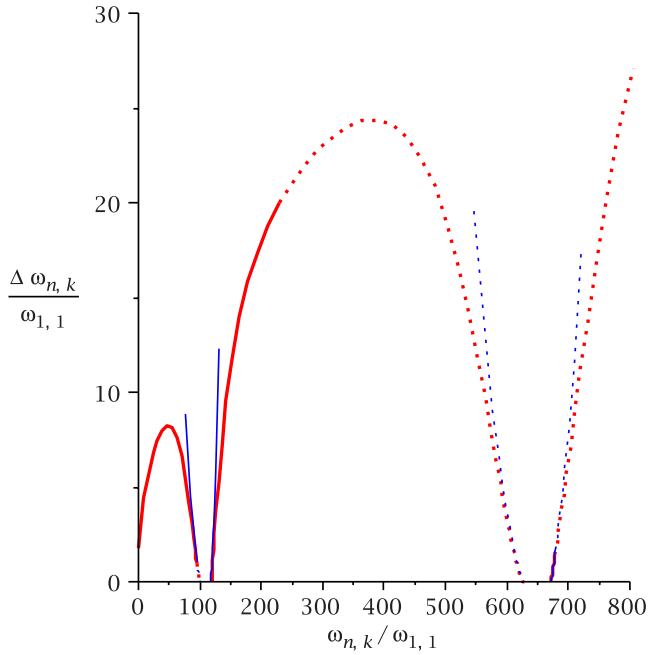

FIG. 3. (Color online) In red, frequency spacing, $(\omega_{n+1,k}-\omega_{n,k})/\omega_{1,1}$ vs frequency for the same parameters, as in Fig. 2. In blue, analytical results obtained from Eq. (29). Curves are solid for $n<N$ and dotted for $n>N$.

band contains all possible values of β_n, $1\leqslant n\leqslant\infty$, i.e., all possible modal shapes for the central beam, $Y_n(u)$. Even though modes with the same shape $Y_n(u)$ repeatedly appear within each band, they differ from band to band because their cantilever continuum, $H_{n,k}(u,v)$, depends on $\gamma_{n,k}$ that is on both n and k [see Eq. (19)]. Note also that within a given band, the frequency increases with the excitation level of the central beam.

At midband, modal frequencies are somewhat sparse and more regularly spaced than at the boundaries. This is confirmed in Fig. 3 that displays the normalized spacing between two consecutive frequencies versus the normalized frequency itself. Notice that the inverse of this function is nothing but the normalized "density of states" of the spectrum. Midband frequencies can be approximately evaluated once we note that the function $A_2(\gamma)$ appearing in secular Eq. (22) is small away from the boundaries $\gamma_{\infty,k}$ given by Eq. (27) and increases slowly and regularly in this region. Rewriting Eq. (22) as $\mu^4-\beta_n^4+4\alpha NA_2(\mu l/L)\mu^3=0$, we seek a solution close to $\mu\sim\beta_n$. With a first Newton iteration we obtain

$$\gamma_{n,k}\simeq\gamma_n^{(0)}\left[1-\frac{\alpha NA_2(\gamma_n^{(0)})}{\beta_n+3\alpha NA_2(\gamma_n^{(0)})+\alpha N\beta_n\dfrac{1}{L}A_2'(\gamma_n^{(0)})}\right],$$

$$|\beta_n-\mu_k^*|\ll\frac{L\Delta_k}{2l},\tag{29}$$

where $\gamma_n^{(0)}=\beta_n l/L$, $\alpha=w/W$, and $A_2(\gamma)$ is given in Eq. (20). In the last equation, $\Delta_k=\gamma_{\infty,k}-\gamma_{1,k}$ is the width of band k and μ_k^* is determined as the solution to $A_2(\mu_k^* l/L)=0$. For k large enough, $\mu_k^*\simeq(k-1/4)\pi L/l$, $k\geqslant 1$. In this case, we have also $\beta_n\simeq(n+1/2)\pi$, $n\geqslant 1$. Approximating the bandwidth by $\Delta_k\simeq\gamma_{\infty,k}-\gamma_{\infty,k-1}\simeq\pi$ as k is large enough, the condition of Eq. (29) becomes $|(n+1/2)l/L-(k-1/4)|\ll 1/2$, which provides bounds on the beam excitation (n) of band k for which Eq. (29) is valid. In this case Eq. (29) simplifies to

$$\gamma_{n,k}\simeq\frac{l}{L}\left[\beta_n-\alpha NA_2\left(\frac{\beta_n l}{L}\right)\right],\quad|\beta_n-\mu_k^*|\ll\frac{L\Delta_k}{2l}.\tag{30}$$

Although simple, this last expression is not very accurate for the first bands.

Very few of the many frequencies occurring in the spectrum of the CM can be detected experimentally. This is mainly due to the modal response of the structure, which for a given driving power, is drastically suppressed as its excitation level increases as we shall prove in the study of a damped driven antenna done in Sec. IV. Moreover, the antenna is generally driven by a harmonic force that is constant over the beam which does not allow for the observation of antisymmetric modes $Y_n(u)$ with n even. In what follows, we show how to evaluate the frequency of the fundamental mode of the structure and explain the clustering phenomenon observed at both edges of each band.

B. Fundamental mode: Mass loading

If a small solution to Eq. (25) exists, $\gamma\ll 1$, we can obtain its approximate expression by expanding Eq. (25) around $\gamma=0$. In this case we find that

$$\gamma\simeq\left(\frac{\mu_b}{\mu_a}\right)^{1/4}\frac{l\beta}{L},\tag{31}$$

where $\mu_a=(m_b+2Nm_t)/L$ is the mass per unit length of the entire antenna (beam plus cantilevers). Replacing this result in Eq. (26) and using the fact that $(\mu_t\mathcal{E}_b)/(\mu_b\mathcal{E}_t)=1$ [see Eqs. (5) and (6)] yields

$$\omega\simeq\sqrt{\frac{\mathcal{E}_b}{\mu_a}}\left(\frac{\beta}{L}\right)^2.\tag{32}$$

In this limit, the inertia of the cantilevers is negligible and the frequency of the vibrational mode is the frequency of a clamped-clamped beam whose mass per unit length includes the mass of the central beam plus the mass of the cantilevers. According to Eqs. (19) and (20), the mode shape $H(u,v)$ corresponding to this small γ solution is found to be

$$H(u,v)\simeq\frac{\gamma^4}{24}v^2(v^2-4v+6)Y(u).\tag{33}$$

Notice that this function is proportional to γ^4 and is very small. This confirms that the cantilevers hardly move at all and that their mass only loads the central beam. Finally, given our parameters, the condition $\gamma\ll 1$ is typically satisfied for the first positive root of Eq. (25) when $\beta=\beta_1$. It is then valid for $\gamma_{1,1}$, i.e., for the fundamental mode. Indeed, using Eq. (31) and the antenna parameters of Sec. II A, we find $\gamma_{1,1}\simeq 0.187\,415\,0\cdots$ while the exact numerical value reads $\gamma_{1,1}=0.187\,413\,6\cdots$, i.e., a relative error of $7\times 10^{-4}\%$.

C. Frequency clustering

The *frequency clustering* evoked in Sec. III A, which has also been observed numerically in three-dimensional (3D) finite-element simulations, can be explained with the help of secular Eq. (22). To evaluate the accumulation of frequencies occurring at the upper edge of the kth band ($\omega_{\infty,k}$) and at the lower edge of the $(k+1)$th band, we seek a perturbative solution of Eq. (22) around $\gamma \sim \gamma_{\infty,k}$ given in Eq. (27). Using Eq. (25) and $\gamma_{n,\bar{k}} \simeq \gamma_{\infty,k} - Q(\gamma_{\infty,k},\beta_n)/Q'(\gamma_{\infty,k},\beta_n)$, where $\bar{k}$ stands either for k or $k+1$, and Q' is the derivative of Q with respect to γ, we obtain

$$\gamma_{n,\tilde{k}} \simeq \gamma_{\infty,k} + \left\{ \frac{L\gamma_{\infty,k}}{2\alpha Nl}\left(\frac{t_{\gamma_{\infty,k}} - \mathrm{th}_{\gamma_{\infty,k}}}{t_{\gamma_{\infty,k}} + \mathrm{th}_{\gamma_{\infty,k}}}\right)\left[1 - \left(\frac{l\beta_n}{L\gamma_{\infty,k}}\right)^4\right] + \mathrm{th}_{\gamma_{\infty,k}} - \frac{2}{t_{\gamma_{\infty,k}} + \mathrm{th}_{\gamma_{\infty,k}}} + \frac{1}{\gamma_{\infty,k}} \right\}^{-1}, \tag{34}$$

where $t_\gamma = \tan\gamma$ and $\mathrm{th}_\gamma = \tanh\gamma$. This solution is valid as far as the corrective term is very small compared to $\gamma_{\infty,k}$. This leads to the two conditions below.

1. Upper band edge

With respect to the frequency clustering at the upper band edge of the kth band, Eq. (34) starts to be valid as soon as β_n is large enough. In this case, it is easy to see that this approximately leads to the condition

$$\beta_n \gg \frac{L\gamma_{\infty,k}}{l}\left(1 + \frac{2\alpha Nl}{L}\right)^{1/4}. \tag{35}$$

This condition can always be satisfied for large enough n, given that in this case, $\beta_n \simeq (n+1/2)\pi$ [for simplicity, we have discarded the term $(t_{\gamma_{\infty,k}} - \mathrm{th}_{\gamma_{\infty,k}})/(t_{\gamma_{\infty,k}} + \mathrm{th}_{\gamma_{\infty,k}})$ that is close to unity]. The longer the cantilever, the easier condition (35) is to be satisfied. For an antenna structure with high cantilever to beam length ratio, we may expect to observe a clustering of modes around the frequency determined in Eq. (28). Experimentally, however, this very much depends on the sensitivity of the measuring device given that highly excited modes for the beam are difficult to detect. Moreover, the range of validity of our model, determined by the condition $n < N$, restricts the possibility of observing the beginning of an upper edge clustering to the fundamental band.

Provided Eq. (35) is satisfied, Eq. (34) simplifies to

$$\gamma_{n,k} - \gamma_{\infty,k} \simeq \frac{NR\gamma_{\infty,k}^3}{\beta_n^4}\left(\frac{\mathrm{th}_{\gamma_{\infty,k}} + t_{\gamma_{\infty,k}}}{\mathrm{th}_{\gamma_{\infty,k}} - t_{\gamma_{\infty,k}}}\right) = -\frac{NR\gamma_{\infty,k}^3}{\beta_n^4}\left(\frac{\mathrm{th}_{\gamma_{\infty,k}} + t_{\gamma_{\infty,k}}}{\mathrm{th}_{\gamma_{\infty,k}} t_{\gamma_{\infty,k}}}\right)^2. \tag{36}$$

The second equality has been obtained from Eq. (27). As we can see, the corrective term to $\gamma_{\infty,k}$ is always negative which confirms that the frequencies are indeed accumulating at the upper edge of the band as n increases. It is also possible to show that the (adequately normalized) modal shape of the cantilever corresponding to $\omega_{n,k}$ factorizes asymptotically as the product of the kth mode of a simple cantilever by the nth mode of a clamped-clamped beam, $H_{n,k}(u,v) \sim \phi_k(v)Y_n(u)$ as $n \to \infty$. Thus, as the excitation of the beam becomes high enough, the modal shape of the antenna is given by a simple cantilever mode modulated by the profile of the central beam. The same result is obtained for a weakly dissipative driven antenna in Sec. IV C.

2. Lower band edge

A frequency clustering at the lower edge of each band does not always occur. This essentially depends on the geometry of the antenna. For the correction given in Eq. (34) to be valid,

$$\beta_n \ll \frac{L\gamma_{\infty,k}}{l}\left[1 - \frac{2\alpha Nl}{L}\left(\frac{\mathrm{th}_{\gamma_{\infty,k}} + t_{\gamma_{\infty,k}}}{\mathrm{th}_{\gamma_{\infty,k}} - t_{\gamma_{\infty,k}}}\right)\right]^{1/4} \tag{37}$$

has to be satisfied. For large cantilever to beam length ratio, however, inequality (37) cannot be satisfied because the square-bracketed term becomes negative. This means either that expanding the secular equation around the upper edge of the kth band does not provide any reliable information on the lower edge of the $(k+1)$th band or simply that no clustering occurs at the lower band edge. For the geometry of the antenna described in Sec. I, frequency clustering occurs and the band gap $\Delta_{k,k+1}$ between the kth and $(k+1)$th bands can be accurately evaluated with the help of Eq. (34) as

$$\Delta_{k,k+1} \equiv \gamma_{1,k+1} - \gamma_{\infty,k}. \tag{38}$$

This expression is accurate to less than 5% for the first gap and to less than 0.5% for the second one and its accuracy improves drastically as k increases.

D. Energy

1. Modal energy

Using expressions (11) and (14)–(24), we can evaluate the energy $E_{n,k}$ of the mode $\varphi_{n,k} = [y_n(x,t), \eta_{n,k}(x,\xi,t)]^T$. After some algebra, we find

$$E_{n,k} = \frac{M_{n,k}A^2\omega_{n,k}^2}{2}, \tag{39}$$

where

$$M_{n,k} = m_b + 2Nm_tL_{n,k}. \tag{40}$$

The quantity $L_{n,k}$ that takes into account the dynamics of the cantilevers at the level of the effective mass $M_{n,k}$ is given by $L_{n,k} = L(\gamma_{n,k})$, where defining $h(v) \equiv \tilde{H}(v) + 1$,

$$L(\gamma) = \int_0^1 h^2(v)dv = \frac{1}{4}\left(\frac{\cos\gamma + \cosh\gamma}{1 + \cos\gamma\cosh\gamma}\right)^2 + \frac{3}{2}\frac{A_2(\gamma)}{\gamma}. \tag{41}$$

Incidentally, we also note a relation that will prove useful when dealing with the motion of a driven weakly damped structure in Sec. IV E,

$$L(\gamma) = \frac{1}{2\gamma^3}\frac{d}{d\gamma}[\gamma^3 A_2(\gamma)]. \tag{42}$$

Equation (39) is exactly the energy of an effective harmonic oscillator with amplitude A, frequency $\omega_{n,k}$, and mass $M_{n,k}$. Notice that according to our definition of $Y(u)$ in Eq. (23), the amplitude is defined as $A^2=\int_0^1 Y_n^2(u)du$ which is independent of n and k. Other definitions of the amplitude (such as the maximal deflection of the central beam at the mid point, for example) are typically mode dependent and redefine the effective mass of the structure. As we see, the effective mass of the antenna is renormalized by the factor $L_{n,k}$ that affects the total mass of the cantilevers, $2Nm_t$. In the specific case of the fundamental mode, we have shown in the previous section that $\gamma_{1,1} \ll 1$. Therefore, $L_{1,1} \simeq 1$ and the effective mass of the antenna, $M_{1,1} \simeq m_b + 2Nm_t$, is its actual mass. This confirms the finding of Sec. III B that in the fundamental mode the cantilevers have a pure mass loading effect. We can also use Eq. (39) to define an effective mode-dependent spring constant $\kappa_{n,k}$ as

$$\kappa_{n,k} = M_{n,k}\omega_{n,k}^2. \tag{43}$$

Once again, this result depends on the definition chosen for the amplitude and is valid here for $A^2=\int_0^1 Y_n^2(u)du$.

E. Fundamental and first collective modes: Comparison with finite-element results

In this section, we compare the results of our CM to those obtained with a FE method that treats the vibrations of the antenna within the frame of 3D elasticity theory. We are primarily interested in the fundamental and first collective modes that are in the first modes of the first and second bands, respectively. These modes are easy to observe experimentally. They are related to the parameters $\gamma_{1,1}$ and $\gamma_{1,2}$, respectively. Using Eq. (25) and the antenna parameters given in Sec. II A, we find that the two first roots of $Q(\gamma,\beta_1)$ with $\beta_1 = 4.730\,04\cdots$ are $\gamma_{1,1} = 0.187\,413\cdots$ and $\gamma_{1,2} = 2.046\,440\cdots$. If we use Eq. (31), one finds $\gamma_{1,1} \simeq 0.187\,415$. It shows that this approximate solution is very reliable for the fundamental frequency. The corresponding frequency, obtained from Eq. (26), is $f_{1,1} = \omega_{1,1}/2\pi \simeq 24.7$ MHz, slightly higher than the frequency observed in simulations (23.6 MHz). This might be explained by the effective cross-sectional stiffness that we approximate for the two material layers. The frequency of the first collective mode calculated from $\gamma_{1,2} = 2.046\,440$ is $f_{1,2} \simeq 2.94$ GHz which is much higher than $f_{1,2}^{\mathrm{FE}} \simeq 1.51$ GHz, the frequency from FE simulations. A reason for this discrepancy is that all elements of the antenna structure are considered as one dimensional in our model. Consequently, their length is the only dimension taken into account in the dynamics of the system. However, in the real structure, the central beam has a nonzero width, W, on the order of the cantilever length, l. For motions of the cantilevers comparable to the beam's, the shear momentum they exert on both of its sides becomes large enough to bend it *laterally* with respect to its midline, an occurrence indeed confirmed by our 3D FE simulations. In first approximation, we can account for this effect by assigning to the cantilevers an effective *dynamical* length ranging from their actual length, l, for small amplitude motions to $l+W/2$, for large ones. If we carry out the substitution $l \to l+W/2$ in $Q(\gamma,\beta_1)$ and re-evaluate $\gamma_{1,2}$, we find $\gamma_{1,2} = 2.085\,115$ and a frequency $f_{1,2} \simeq 1.55$ GHz, within 3% of the simulated value.

The shapes of the central beam predicted by the CM are the same for the fundamental and first collective modes. They are given by $Y_1(u)$, obtained from Eq. (23) for $\beta=\beta_1$. The shapes of the cantilever continua, however, are different and given by Eq. (19) as $H_{1,1}(u,v)$ and $H_{1,2}(u,v)$, respectively. A comparison of these results to those of the FE simulation is done in Fig. 4. The FE and CM results for the fundamental and first collective modes are given in the upper left and upper right panels, respectively. As indicated, the FE result is to the right of the CM result. In both cases, the color code indicates the displacement (amplitude) of the elements with respect to the clamps of the central beam (i.e., its extremities). For the CM results, only half of the absolute displacement of the cantilever continuum, $Y_1(u)+H_{1,k}(u,v)$, $k=1,2$, $v \geqslant 0$, is displayed. For $v=0$, this displacement is precisely the beam's, $Y_1(u)$. As we see, the CM predictions are in excellent agreement with the FE results. For both the fundamental and the first collective modes, the shape of the central beam is in the fundamental mode of a bare beam, $Y_1(u)$. In the fundamental mode, the deflection of the cantilever continuum with respect to the beam is imperceptible as predicted by the CM in the small γ limit (see Sec. III B). Indeed, from Eq. (33), we have $H_{1,1}(u,v) \propto \gamma_{1,1}^4 Y_1(u)$, which means that the continuum deflection is roughly 5000 times smaller than that of the beam. This is markedly different for the first collective mode where the motion of the continuum is on the order of the beam amplitude as seen on the upper right panel. Note that if their amplitudes are very different, the actual shapes of the continua for the fundamental and first collective modes are similar and are given to a very good approximation by the fundamental mode of a bare cantilever. This somewhat surprising fact becomes clear on the modal expansion of the cantilever continuum, $H_{n,k}(u,v) \equiv \tilde{H}_{n,k}(v)Y_n(u)$. Introducing the normalized cantilever modes, $\psi_l(v)$, satisfying $\psi_l^{(iv)}(v) = \gamma_{\infty,l}^4 \psi_l(v)$, we obtain from Eq. (16),

$$\tilde{H}_{n,k}(v) = \sum_{l=1}^{\infty} \frac{\gamma_{n,k}^4 \Psi_l}{\gamma_{\infty,l}^4 - \gamma_{n,k}^4}\psi_l(v), \tag{44}$$

with $\Psi_l = \int_0^1 \psi_l(v)dv = -(2/\gamma)(\cos\gamma + \cosh\gamma)/(\sin\gamma + \sinh\gamma)$, where $\gamma = \gamma_{\infty,l}$. Now, we have seen in Sec. III C that for $k \geqslant 2$, $\gamma_{n,k}$ is very close to $\gamma_{\infty,k-1}$. According to Eq. (44), this means that the mode selected for the cantilever continuum is $\psi_{k-1}(v)$. In particular, for the first collective mode, $\gamma_{1,2}$, the continuum adopts basically the shape of the *fundamental* cantilever mode, $\psi_1(v)$. For the modes of the fundamental band ($k=1$), this is also the fundamental cantilever mode that is predominantly excited even if its amplitude is so small compared to the beam's that the cantilevers seem flat at the scale of the figure.

To analyze further the similarities between the FE and CM results, the first excited modes of the fundamental and collective bands are displayed in the lower left and right

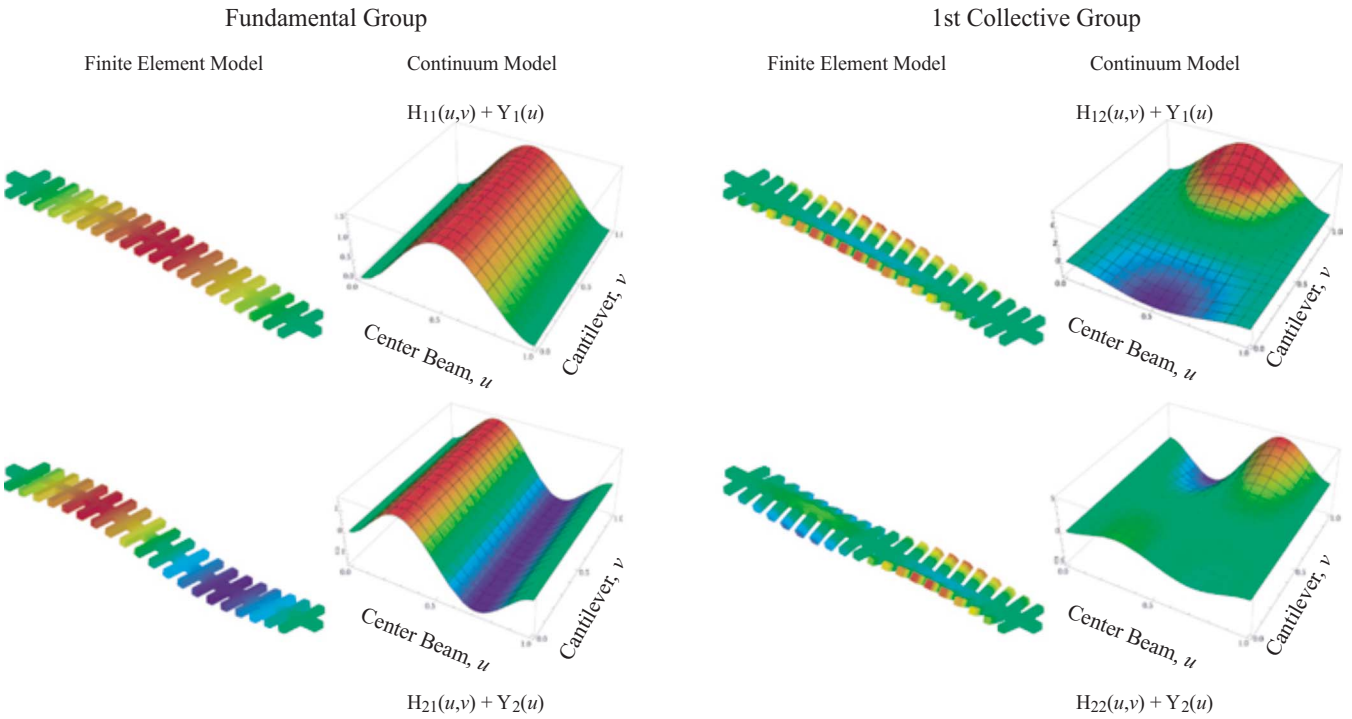

FIG. 4. (Color online) Comparison between FE and CM results for the fundamental mode (upper left panel), the first excited mode of the fundamental group (lower left panel), the first collective mode (upper right panel), and the first excited collective mode (lower right panel). The parameters for the antenna structure are those quoted in Sec. II A.

panels of Fig. 4, respectively. We clearly observe in both cases that the beam deflection is in the first excited mode of a bare beam, $Y_2(u)$, as predicted by the CM. Moreover, as for the fundamental mode, the cantilevers of the first excited mode of the fundamental group are hardly moving. Evaluating the first root of $Q(\gamma,\beta_2)=0$ with $\beta_2=7.853\,20\cdots$ yields $\gamma_{2,1}=0.311\,14\cdots$. This is small enough for the results of Sec. III B to hold. Indeed, expression (31) gives $\gamma_{2,1}\simeq 0.311\,16\cdots$. Therefore, the continuum deflection can safely be evaluated from Eq. (33) and we find that it is roughly 100 times smaller than the beam deflection, which explains that no cantilever motion can be detected in the FE results. Once again, this is markedly different for the first excited mode of the collective group whose cantilevers, according to the FE results, are experiencing a deflection comparable to the beam amplitude in full agreement with the predictions of the CM. Note that for this two first excited modes of the fundamental and collective bands, the cantilever deflections adopt the shape of the fundamental mode of a bare cantilever, $\psi_1(v)$, as indicated by modal expansion (44).

Even though one dimensional in essence, the CM gives a good qualitative understanding of the modes of the 3D antenna. It correctly reproduces the modal shapes of the central beam and the cantilevers observed in the FE simulation and is able to explain the frequency clustering occurring in the spectrum of the structure. We use it in the next section as the basic model in the investigation of the effect of a two-frequency driving on the response of a weakly nonlinear and dissipative antenna.

IV. DRIVEN DAMPED SYSTEM

We conclude this section devoted to the linear system by calculating the exact solution of a damped antenna structure driven by a spatially uniform harmonic force density, $f(t)$, in the continuum approximation. This force density can, for instance, be exerted by an external magnetic field, B, orthogonal to the flexural vibrations of the central beam, acting on an ac with frequency ω_d passed through the thin layer of gold coating the structure. The beam vibrations then generate in turn an electromotive voltage $V_{\mathrm{emf}}(t)$ at the clamped ends of the antenna that is proportional to the rate of change in the magnetic flux,

$$V_{\mathrm{emf}}(t) = B\int_0^L \frac{\partial y(x,t)}{\partial t}dx. \tag{45}$$

Ultimately, this voltage can be monitored to determine the motion of the central beam of the structure and to derive its "spectrum," i.e., the time root mean square of the induced voltage, $\sqrt{\langle V_{\mathrm{emf}}^2(t)\rangle}$, versus the driving frequency, ω_d. This detection scheme has been used in the previously reported experimental measurements of the antenna resonators in Refs. 12 and 20. Other activation/detection schemes such as electrostatic, piezoelectric, and optical are also typically sensitive to the average transverse displacement of resonating elements, and the following analysis applies quite generally.

A. Model

Supplementing the equations of motions (7) and (8) with damping and driving terms we obtain

$$\mathcal{E}_b\frac{\partial^4 y}{\partial x^4} + \mu_b\frac{\partial^2 y}{\partial t^2} + \nu_b\frac{\partial y}{\partial t} = -\frac{2\mathcal{E}_t N}{L}\left.\frac{\partial^3 \eta}{\partial \xi^3}\right|_{\xi=0} + f(t), \tag{46}$$

$$\mathcal{E}_t \frac{\partial^4 \eta}{\partial \xi^4} + \mu_t \frac{\partial^2 \eta}{\partial t^2} + \nu_t \frac{\partial \eta}{\partial t} = -\mu_t \frac{\partial^2 y}{\partial t^2} - \nu_t \frac{\partial y}{\partial t}. \tag{47}$$

Boundary conditions for the beam and cantilever deflections are the same as in Eqs. (9) and (10). The harmonic force density is given by $f(t)=f\cos(\omega_d t)$. Note that in Eq. (47), the damping term affecting the cantilevers involves their absolute displacement, $y(x,t)+\eta(x,\xi,t)$, rather than their relative displacement, $\eta(x,\xi,t)$. The choice of an appropriate damping term depends of course on the type of damping experienced by the structure. To simplify, we consider here that damping occurs through air friction and is then proportional to the absolute velocity of the cantilevers. Moreover, it is proportional to the surface in contact with the ambient air. For that reason, the damping per unit length is proportional to the width of the element involved and then $\nu_t/\nu_b = w/W = \mu_t/\mu_b = \mathcal{E}_t/\mathcal{E}_b$. Material damping, whether of the viscoelastic or hysteretic type (see for instance Ref. 28), would essentially affect the rigidities of Eqs. (46) and (47) in such a way that $\mathcal{E}$ is replaced by $\mathcal{E}+\mathcal{E}^*\partial/\partial t$. The exact solution of systems (46) and (47) can still be obtained in this case.

B. Exact solution

Introducing the Fourier transform $\tilde{g}(\omega)=\int dt e^{i\omega t} g(t)$ and its inverse $g(t)=\int d\omega e^{-i\omega t}\tilde{g}(\omega)/(2\pi)$, and using the dimensionless quantities defined in Eq. (13), we can cast Eqs. (46) and (47) into

$$\frac{\partial^4 \tilde{y}}{\partial u^4} - \mu_c^4 \tilde{y} = -NR \left.\frac{\partial^3 \eta}{\partial v^3}\right|_{v=0} + \bar{F}(\omega), \tag{48}$$

$$\frac{\partial^4 \tilde{\eta}}{\partial v^4} - \gamma_c^4 \tilde{\eta} = \gamma_c^4 \tilde{y}, \tag{49}$$

where $F(t)=F\cos(\omega_d t)$ with $F=L^4 f/\mathcal{E}_b$ and

$$\gamma_c^4 = \frac{l^4}{\mathcal{E}_t}(\mu_t \omega^2 + i\nu_t \omega),$$

$$\mu_c^4 = \frac{L^4}{\mathcal{E}_b}(\mu_b \omega^2 + i\nu_b \omega) = \left(\frac{L\gamma_c}{l}\right)^4. \tag{50}$$

These last parameters are the complex version (because of the presence of damping) of the parameters μ and γ defined in Eq. (13). Note also that F has the dimension of a length. As in the earlier case, we can solve Eq. (49) with its boundary conditions

$$\tilde{\eta}(u,v,\omega) = \tilde{H}(v,\omega)\tilde{y}(u,\omega), \tag{51}$$

where

$$\tilde{H}(v,\omega) = [A_1(\gamma_c)\cos(\gamma_c v) + A_2(\gamma_c)\sin(\gamma_c v) + A_3(\gamma_c)\cosh(\gamma_c v) + A_4(\gamma_c)\sinh(\gamma_c v) - 1]. \tag{52}$$

The coefficients A_i are the same as those given in Eq. (20). Reinstating this expression in Eq. (48), we finally obtain

$$\frac{\partial^4 \tilde{y}(u,\omega)}{\partial u^4} - \beta_c^4 \tilde{y}(u,\omega) = \tilde{F}(\omega), \tag{53}$$

where

$$\beta_c^4 = \mu_c^4 + \gamma_c^3 RN \frac{\cos\gamma_c \sinh\gamma_c + \sin\gamma_c \cosh\gamma_c}{1+\cos\gamma_c \cosh\gamma_c}, \tag{54}$$

which is the complex analog of secular Eq. (22). Finally, applying the appropriate boundary conditions to $\tilde{y}(u,\omega)$ we can, after some algebra, cast the solution to Eq. (53) into

$$\tilde{y}(u,\omega) = \left\{ T(\beta_c)\left[\frac{\cos[\beta_c(u-1/2)]}{\sin(\beta_c/2)} + \frac{\cosh[\beta_c(u-1/2)]}{\sinh(\beta_c/2)} \right] - 1 \right\} \frac{\tilde{F}(\omega)}{\beta_c^4}, \tag{55}$$

where we have defined

$$T(\beta_c) = \frac{\tan(\beta_c/2)\tanh(\beta_c/2)}{\tan(\beta_c/2)+\tanh(\beta_c/2)}. \tag{56}$$

Now, the driving $f(t)$ being harmonic, we have $\tilde{F}(\omega) = F\pi[\delta(\omega-\omega_d)+\delta(\omega+\omega_d)]$ and noticing that the sign inversion $\omega \to -\omega$ amounts to taking the complex conjugate, we finally obtain

$$y(x,t) = F\,\mathrm{Re}\left\{ \frac{e^{-i\omega_d t}}{\beta_c^4}\left[T(\beta_c)\left(\frac{\cos[\beta_c(u-1/2)]}{\sin(\beta_c/2)} + \frac{\cosh[\beta_c(u-1/2)]}{\sinh(\beta_c/2)} \right) - 1 \right] \right\}. \tag{57}$$

Expression (55) makes it clear that the shape of the central beam induced by the force density $f(t)$ is symmetric with respect to its midpoint, $u=1/2$. This is expected as the force density itself possesses this symmetry. Consequently, none of the antisymmetric modes of the central beam are excited by this method. Moreover, in presence of dissipation, the beam shape never corresponds to an exact symmetric modal shape even when the driving frequency is one of the structure modal frequencies. We can see that for weak dissipation, however, the denominator of $T(\beta_c)$ becomes small (on the order of ν_t) when $\omega_d \sim \omega_{2n+1,k}$. This is because the solutions to $\tan(x/2)+\tanh(x/2)=0$ are precisely the β_{2n+1}'s. This eventually leads $y(x,t)$ to assume a shape close to the mode $Y_{2n+1}(u)$.

C. Modal expansion

As we have seen earlier, the modes of the antenna structure are such that the central beam possesses the *exact* shape of a clamped-clamped mode, $Y_n(u)$ [see Eq. (23)]. However, the force $f(t)$ applied to the beam excites now *all* symmetric clamped-clamped modes. To get a sense of which modes are predominantly excited, we first expand the Fourier transform of the deflection as $\tilde{y}(u,\omega)=\Sigma_n \tilde{y}_n(\omega)Y_n(u)$, insert it in Eq. (53), solve for $\tilde{y}_n(\omega)$ and finally obtain

$$y(x,t) = F\sum_{n=0}^{\infty} \frac{\Gamma_{2n+1}\cos[\omega_d t + \vartheta_{2n+1}(\omega_d)]}{|\beta_c^4(\omega_d) - \beta_{2n+1}^4|} Y_{2n+1}(u), \quad (58)$$

where $\Gamma_n = \int_0^1 Y_n(u)du$ and where $\vartheta_n(\omega) = \arg[\beta_c^4(\omega) - \beta_n^4]$. The reason why the sum runs exclusively over odd numbers in Eq. (58) is because integrals of antisymmetric clamped-clamped modes, Γ_{2n}, vanish which confirms that none of them is excited by $f(t)$. For symmetric modes, a simple calculation yields $\Gamma_{2n+1} = 4\tan(\beta_{2n+1}/2)/\beta_{2n+1}$. Clearly, expression (58) shows that the mode $Y_{2n+1}(u)$ is singled out when the driving frequency is close to one of the modal frequencies $\omega_{2n+1,k}$ and the dissipation is weak enough $[|\beta_c^4(\omega_d) - \beta_{2n+1}^4| \propto \nu_t$ in this case, see Sec. IV E].

Also of interest is the modal expansion of the cantilever continuum. Introducing the normalized cantilever modes, $\psi_k(v)$, $k \geqslant 1$, satisfying $\psi_k^{(iv)}(v) = \gamma_{\infty,k}^4 \psi_k(v)$, we can expand $\tilde{H}(v,\omega)$ in Eq. (52) as $\tilde{H}(v,\omega) = \Sigma_k \tilde{H}_k(\omega)\psi_k(v)$ uses Eq. (51) and insert it in Eq. (49), and finally solve for $\tilde{H}_k(\omega)$. This yields

$$\tilde{H}(v,\omega) = \sum_{k=1}^{\infty} \frac{\gamma_c^4(\omega)\Psi_k}{\gamma_{\infty,k}^4 - \gamma_c^4(\omega)}\psi_k(v), \quad (59)$$

where $\Psi_k = \int_0^1 \psi_k(v)dv = -(2/\gamma)(\cos\gamma + \cosh\gamma)/(\sin\gamma + \sinh\gamma)$, where $\gamma = \gamma_{\infty,k}$. Hence, $\Psi_k \simeq -2/\gamma_{\infty,k}$, as k becomes large. The interesting point about this calculation is to show what cantilever mode is selected according to the driving frequency. When the latter is close to the modal frequency $\omega_{n,k}$ with n small, and provided that the dissipation is weak enough, $\gamma_c(\omega_{n,k}) \simeq \gamma_{n,k}$. Now, we have seen in Sec. III C that for $k \geqslant 2$, $\gamma_{n,k}$ is very close to $\gamma_{\infty,k-1}$. According to Eq. (59), this means that for $\omega_d \sim \omega_{n,k}$, the mode selected for the cantilever continuum is $\psi_{k-1}(v)$. In particular, if the system is driven near the first *collective* mode frequency, $\omega_{1,2}$, the continuum adopts basically the shape of the fundamental cantilever mode. Note that for driving frequencies in the fundamental band ($k=1$), this is always the fundamental cantilever mode that is predominantly excited. For other bands ($k \geqslant 2$), the continuum interpolates between the shape of the mode $\psi_{k-1}(v)$ close to the lower band edge and $\psi_k(v)$ close to the upper band edge. In practice, however, as our model provides consistent results for $n < N$ only, the range of physically relevant frequencies is restricted to the lower band edge. For all peaks but those of the fundamental band, therefore, the relevant modes of the structure at frequency $\omega_{n,k}$ are $Y_n(u)$ and $\psi_{k-1}(v)$.

D. Amplitude-frequency spectrum

Most of the time, this is not the beam deflection $y(x,t)$ but rather its average over the beam length (or its time derivative, see below) that is detected. For that reason, we define

$$\bar{y}(t) \equiv \frac{1}{L}\int_0^L y(x,t)dx. \quad (60)$$

Using expression (57), we immediately obtain

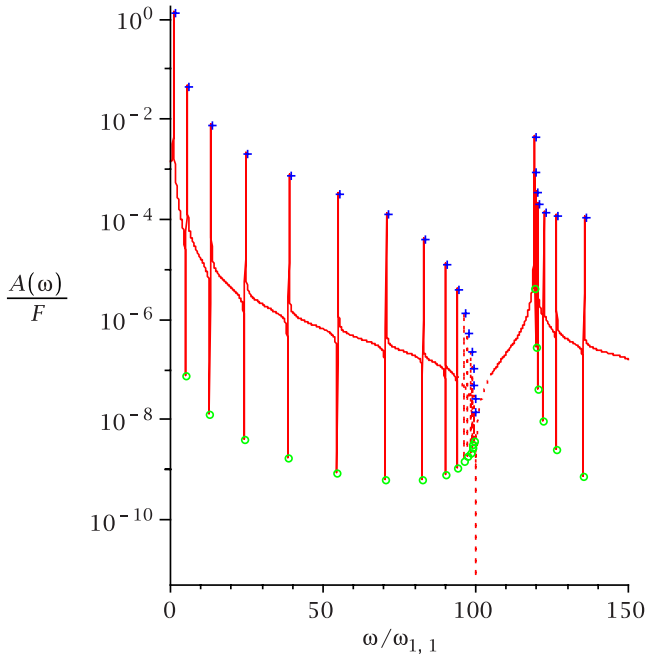

FIG. 5. (Color online) (a) Amplitude-frequency spectrum, ($\mathcal{A}(\omega)/F$ vs $\omega/\omega_{1,1}$), obtained from Eq. (62) for $N=20$ and the antenna parameters given in Sec. II A. Solid lines correspond to $n<N$ (physically relevant frequencies) and the dotted one to $n>N$. (b) Zoom in the region of the first collective frequency peak. For both (a) and (b), analytical results for peaks (+) and dips (○) are obtained from Eqs. (65) and (66), respectively.

$$\bar{y}(t) = \mathcal{A}(\omega_d)\cos[\omega_d t - \theta(\omega_d)], \quad (61)$$

where the amplitude $\mathcal{A}(\omega)$ and the phase $\theta(\omega)$ are, respectively, given by

$$\mathcal{A}(\omega) = \frac{F}{|\beta_c^4|}\left|\frac{4T(\beta_c)}{\beta_c} - 1\right|,$$

$$\theta(\omega) = \arg\left(\frac{1}{\beta_c^4}\left[\frac{4T(\beta_c)}{\beta_c} - 1\right]\right). \quad (62)$$

Figure 5(a) displays the amplitude-frequency spectrum for the antenna parameters given in Sec. II A. Quantities plotted are the dimensionless amplitude, $\mathcal{A}(\omega)/F$, given by Eq. (62), versus the dimensionless frequency $\omega/\omega_{1,1}$. Therefore, the peak of the fundamental is located at 1. The peak of the first collective mode (first frequency of the second band) is approximately located at $\omega_{1,2}/\omega_{1,1} = 119.23$, as seen on Fig. 5(b). The dissipation parameter has been chosen in such a way as to provide a fundamental peak with quality factor $Q = \mu_t\omega_{1,1}/\nu_t$ on the order of $\sim 10^3$, a typical value in experiments. The physically relevant part of the spectrum [corresponding to $n<N$, that is $|\beta_c(\omega)| < (N+1/2)\pi$], is drawn in solid line while the irrelevant part is drawn in dotted line. Because of the weak damping, frequency peaks occur when the driving frequency is close to one of the modal frequencies, $\omega_{2n+1,k}$. As seen in Fig. 5(a), peak amplitudes decrease rapidly as the frequency increases within a given band. However, the first peak of the collective band, approximately located at $\omega_{2,1} \simeq 119.23\omega_{1,1}$, is much higher than the last peaks of the fundamental band. That is why it is easily observed in experiments. An analytical formula for peak heights is ob-

tained in the next section in the weakly dissipative regime.

Also of interest are the dips occurring slightly before the peaks. Their occurrence is due to the fact that at certain frequencies, the integral of the shape of the central beam over its length is close to zero. This is especially important for detection schemes involving an electromotive voltage because the signal is close to zero in this case. For a *nondissipative system*, there are frequencies such that the integral is exactly zero. The shape of the central beam resembles the modal shapes $Y_{2n+1}(u)$, $n \geqslant 1$, in this case. From Eq. (62), we see that spectral dips are given by the simple relation $4T(\beta)=\beta$, where $T(\beta)$ is given in Eq. (56). Denoting with a hat all quantities related to the dips, we can show that the solution of the previous equation reads approximately

$$\hat{\beta}_{2n+1} \simeq \beta_{2n+1} + \frac{4}{4-\beta_{2n+1}}, \quad n \geqslant 1. \tag{63}$$

This explains why dips are close to the frequency peaks. The corresponding frequencies are obtained by solving the secular equation $Q(\gamma, \hat{\beta}_{2n+1})=0$ for γ [see Eq. (25)] whose solutions $\hat{\gamma}_{2n+1,k}$ define $\hat{\omega}_{2n+1,k}=\sqrt{\mathcal{E}_t/\mu_t}(\hat{\gamma}_{2n+1,k}/l)^2$. Last, the deepest dip occurring around 100 in Fig. 5(a) is due to the upper band edge of the fundamental band, obtained in the nondissipative case for $\omega_{\infty,1}/\omega_{1,1}=(\gamma_{\infty,1}/\gamma_{1,1})^2 \simeq 100.103$. Though, this part of the spectrum is not physically relevant.

E. Weak dissipation

Analytical results for weakly dissipative systems are obtained by expanding the quantities of interest around their value in absence of dissipation ($\nu_t=0$). Let us assume that for $\nu_t=0$, ω_0 is the frequency of interest, a modal, or dip frequency, for example. Then $\gamma_0=l(\mu_t\omega_0^2/\mathcal{E}_t)^{1/4}$ and β_0 given by Eq. (22) are real. For $\omega \sim \omega_0$, we have $\beta_c^4(\omega,\nu_t) \simeq \beta_0^4+[(\omega-\omega_0)\,\partial\gamma_c^4/\partial\omega|_0+\nu_t\,\partial\gamma_c^4/\partial\nu_t|_0]\,\partial\beta_c^4/\partial\gamma_c^4|_0$. Now, using Eq. (54) for β_c, Eq. (50) for γ_c and the result obtained in Eq. (42) yields

$$|\beta_c^4(\omega)-\beta_0^4| \simeq \frac{L^4\mu_t}{\mathcal{E}_t}\left[1+\frac{2Nm_t}{m_b}L(\gamma_0)\right] \times \sqrt{4\omega_0^2(\omega-\omega_0)^2+\left(\frac{\nu_t\omega_0}{\mu_t}\right)^2} \quad (\omega \sim \omega_0). \tag{64}$$

Notice that because $\omega \sim \omega_0$, the function under the square root is, in first order in ν_t, equivalent to $(\omega^2-\omega_0^2)^2+(\nu_t\omega/\mu_t)^2$, which is the typical form for a harmonic oscillator. However $\beta_c(\omega,\nu_t)$ has to be expanded up to second order in ν_t and $\omega-\omega_0$ to compute the correct frequency shift induced by the damping because the latter is of order ν_t^2.

By expanding $\beta_c(\omega)$ around β_{2n+1} and using Eq. (62), we find that the amplitude of the peak with frequency $\omega_{2n+1,k}$ is given by $\mathcal{A}(\omega) \simeq 16F\tanh^2(\beta_{2n+1}/2)/[\beta_{2n+1}^2|\beta_c^4(\omega)-\beta_{2n+1}^4|]$. Therefore, from Eq. (64) we obtain the peak height as

$$\mathcal{A}_{m,k}^{\text{peak}} \simeq \frac{16\mathcal{E}_tF}{L^4\nu_t}\left[1+\frac{2Nm_t}{m_b}L(\gamma_{m,k})\right]^{-1}\frac{\tanh^2\left(\frac{\beta_m}{2}\right)}{\beta_m^2\omega_{m,k}}, \tag{65}$$

where $m=2n+1$, $n \geqslant 0$. In the same way, expanding $\beta_c(\omega)$ around $\hat{\beta}_{2n+1}$ [see Eq. (63)] we can show after some algebra that the amplitude of a dip with frequency $\hat{\omega}_{2n+1,k}$ is given by $\mathcal{A}(\omega) \simeq F/4\hat{\beta}_{2n+1}^8[(\hat{\beta}_{2n+1}/2)/[\tanh(\hat{\beta}_{2n+1}/2)]-1]^2|\beta_c^4(\omega)-\hat{\beta}_{2n+1}^4|$. Hence, the minimum of the dip

$$\mathcal{A}_{m,k}^{\text{dip}} \simeq \frac{FL^4\nu_t}{4\mathcal{E}_t}\left(\frac{\hat{\beta}_m/2}{\tanh(\hat{\beta}_m/2)}-1\right)^2 \times\left[1+\frac{2Nm_t}{m_b}L(\gamma_{m,k})\right]\frac{\tilde{\omega}_{m,k}}{\hat{\beta}_m^8}, \tag{66}$$

with $m=2n+1$, $n \geqslant 1$.

F. Electromotive potential spectrum

From Eqs. (60) and (61), it is now straightforward to evaluate the electromotive potential $V_{\text{emf}}(t)$ given in Eq. (45). It reads

$$\frac{V_{\text{emf}}(t)}{LB}=\frac{d\bar{y}(t)}{dt}=\omega_d\mathcal{A}(\omega_d)\sin[\omega_dt-\theta(\omega_d)-\pi], \tag{67}$$

from which we eventually deduce the time rms

$$\sigma_{\text{emf}} \equiv \sqrt{\langle V_{\text{emf}}^2(t)\rangle}=\frac{BFL\omega_d}{\sqrt{2}}\frac{1}{|\beta_{c,d}^4|}\left|\frac{4T(\beta_{c,d})}{\beta_{c,d}}-1\right|. \tag{68}$$

From the formulas of the previous section we can evaluate the peak maxima and dip minima of the electromotive rms and we are able to compare them with those observed in experiments.

V. CONCLUSION

Here, we have presented the closed-form solution of a CM describing the dynamics of the coupled-beam resonator. The inherent modifications associated with the dynamics of coupled-element structures can be engineered to result in advantageous frequency and amplitude performance, which is otherwise difficult to obtain with simple geometries. In particular, the measurements of a similar nanomechanical fabricated device have been reported previously[12,20,22] to demonstrate some of the highest mechanical resonance frequencies up to 3 GHz, reported to date.

The CM allows for a clear comparison of the modal shapes and spectrum with full FE analysis of the structure. The findings and resulting discussion in Sec. III E elucidate the behavior of the coupled-element system in the fundamental and first collective modes. In particular, it is shown that the enhanced effective amplitude of the collective mode results from the collective excitation of the cantilever continuum at high frequencies, while the supporting central beam effectively adds the cantilever motion by moving in its fundamental mode shape with zero nodes, thus providing maximum transduction of the cantilever displacement to the measured magnetomotive voltage. Investigating further the

dynamical response of the structure to a harmonic driving force has helped elucidate the response of experimentally measured structures.

In brief, the CM proves to be simple enough to be studied analytically and provides results that are accurate enough to reproduce most of the features observed either numerically with a FE method or experimentally. It is therefore of great help in interpreting experimental results. Moreover, its simplicity allows us to investigate the dynamics of weakly nonlinear and damped structures, an asset we shall take advantage of in a forthcoming paper devoted to the study of a recently measured modal coupling occurring in the structure. This analysis that can readily be applied to a general set of weakly damped and nonlinear coupled elements provides insights into the nontrivial modifications of the dynamics of such systems that can be used to carefully engineer them to suit specific technical needs. This is of great importance given the numerous applications of rf MEMS and NEMS devices in the areas of wireless communications and frequency manipulation.

ACKNOWLEDGMENTS

This work was supported by NSF (DMR-0449670).

[1]J. A. Wheeler and W. H. Zurek, *Quantum Theory and Measurement* (Princeton University, Princeton, 1983).
[2]W. Zurek, Rev. Mod. Phys. **75**, 715 (2003).
[3]I. Martin and W. H. Zurek, Phys. Rev. Lett. **98**, 120401 (2007).
[4]C. Caves, K. S. Thorne, R. W. P. Drever, V. D. Sandberg, and M. Zimmermann, Rev. Mod. Phys. **52**, 341 (1980).
[5]M. Bocko and R. Onofrio, Rev. Mod. Phys. **68**, 755 (1996).
[6]H. J. Mamin and D. Rugar, Appl. Phys. Lett. **79**, 3358 (2001).
[7]D. Rugar, R. Budakian, H. J. Mamin, and B. W. Chui, Nature (London) **430**, 329 (2004).
[8]J. Dorignac, A. Kalinowski, S. Erramilli, and P. Mohanty, Phys. Rev. Lett. **96**, 186105 (2006).
[9]V. B. Braginsky and F. Y. Khalili, Rev. Mod. Phys. **68**, 1 (1996).
[10]C. Montemagno and G. Bachand, Nanotechnology **10**, 225 (1999).
[11]G. Wu, H. Ji, K. Hansen, T. Thundat, R. Datar, R. Cote, M. Hagan, A. K. Chakraborty, and A. Majumdar, Proc. Natl. Acad. Sci. U.S.A. **98**, 1560 (2001).
[12]A. Gaidarzhy, G. Zolfagharkhani, R. L. Badzey, and P. Mohanty, Phys. Rev. Lett. **94**, 030402 (2005).
[13]M. D. LaHaye, O. Buu, B. Camarota, and K. C. Schwab, Science **304**, 74 (2004).
[14]P. Mohanty, in *Applications of Nonlinear Dynamics* (Springer) (to be published); P. Mohanty, arXiv:0802.4116v1.
[15]C. T. C. Nguyen, IEEE Trans. Microwave Theory Tech. **47**, 1486 (1999).
[16]C. T. C. Nguyen, L. P. B. Katehi, and G. M. Rebitz, Proc. IEEE **86**, 1756 (1998).
[17]R. Badzey, G. Zolfagharkhani, A. Gaidarzhy, and P. Mohanty, Appl. Phys. Lett. **85**, 3587 (2004).
[18]P. Mohanty, G. Zolfagharkhani, S. Kettermann, and P. Fulde, Phys. Rev. B **70**, 195301 (2004).
[19]X. M. H. Huang, C. Zorman, M. Mehregany, and M. L. Roukes, Nature (London) **421**, 496 (2003).
[20]A. Gaidarzhy, M. Imboden, P. Mohanty, B. Sheldon, and J. Ranken, Appl. Phys. Lett. **91**, 203503 (2007).
[21]F. D. Bannon III, J. R. Clark, and C. T.-C. Nguyen, IEEE J. Solid-State Circuits **35**, 512526 (2000).
[22]A. Gaidarzhy, G. Zolfagharkhani, R. Badzey, and P. Mohanty, Appl. Phys. Lett. **86**, 254103 (2005).
[23]R. Maranganti and P. Sharma, Phys. Rev. Lett. **98**, 195504 (2007).
[24]S. M. Han, H. Benaroya, and T. Wei, J. Sound Vib. **225**, 935 (1999).
[25]A. H. Nayfeh and P. F. Pai, *Linear and Nonlinear Structural Mechanics*, Wiley Series in Nonlinear Science, (Wiley-Interscience, Weinheim, Germany, 2004).
[26]L. A. Segel, *Mathematics Applied to Continuum Mechanics* (Dover, New York, 1987), p. 207.
[27]J. M. Gere and S. P. Timoshenko, *Mechanics of Materials* (PWS, Boston, 1997).
[28]C. V. de Silva, *Vibration: Fundamentals and Practice*, 2nd ed. (CRC, Taylor & Francis, Boca Raton, FL, 2007), p. 385–439.